

This discussion paper is/has been under review for the journal Atmospheric Measurement Techniques (AMT). Please refer to the corresponding final paper in AMT if available.

# Photoacoustic and nephelometric spectroscopy of aerosol optical properties with a supercontinuum light source

N. Sharma<sup>1</sup>, I. J. Arnold<sup>2</sup>, H. Moosmüller<sup>2</sup>, W. P. Arnott<sup>3</sup>, and C. Mazzoleni<sup>1</sup>

<sup>1</sup>Atmospheric Science Program and Physics Department Michigan Technological University, 1400 Townsend Drive, Houghton, MI 49931, USA

<sup>2</sup>Division of Atmospheric Sciences, Desert Research Institute, 2215 Raggio Pkwy, Reno, NV 89512, USA

<sup>3</sup>Physics Department, University of Nevada, 1664 N Virginia St, Reno, NV 89557, USA

Received: 20 June 2013 – Accepted: 23 June 2013 – Published: 11 July 2013

Correspondence to: N. Sharma (noopurs@mtu.edu) and C. Mazzoleni (cmazzoleni@mtu.edu)

Published by Copernicus Publications on behalf of the European Geosciences Union.

## Photoacoustic and nephelometric spectroscopy of aerosol properties

N. Sharma et al.

Title Page

Abstract

Introduction

Conclusions

References

Tables

Figures

⏪

⏩

◀

▶

Back

Close

Full Screen / Esc

Printer-friendly Version

Interactive Discussion

## Abstract

A novel multi-wavelength photoacoustic-nephelometer spectrometer (SC-PNS) has been developed for the optical characterization of atmospheric aerosol particles. This instrument integrates a white light supercontinuum laser with photoacoustic and nephelometric spectroscopy to measure aerosol absorption and scattering coefficients at five wavelength bands (centered at 417, 475, 542, 607, and 675 nm). These wavelength bands were selected from the continuous spectrum of the laser (ranging from 400–2200 nm) using a set of optical interference filters. Absorption and scattering measurements on laboratory-generated aerosol samples were performed sequentially at each wavelength band.

To test the instrument we measured the wavelength dependence of absorption and scattering coefficients of kerosene soot and common salt aerosols. Results were favorably compared to those obtained with a commercial 3-wavelength photoacoustic and nephelometer instrument demonstrating the utility of the SC light source for studies of aerosol optical properties at selected wavelengths. Here, we discuss instrument design, development, calibration, performance and experimental results.

## 1 Introduction

Atmospheric aerosols are major players in determining the Earth's radiation budget (Horvath, 1993). Different particles have different absorption and scattering spectra. For example, soot particles absorb solar radiation over a broad wavelength range from the ultraviolet to the infrared; in contrast, most organic particles absorb weakly in the visible, while brown carbon particles absorb mostly in the UV-blue part of the solar spectrum (Chen and Bond, 2010). Entrained mineral dust particles also exhibit characteristic scattering and absorption spectra depending on their composition (e.g., amount of iron oxides, Moosmüller et al., 2012), size, and morphology. The absorption of solar radiation by these particles contributes to the heating of the surrounding

AMTD

6, 6293–6327, 2013

## Photoacoustic and nephelometric spectroscopy of aerosol properties

N. Sharma et al.

Title Page

Abstract

Introduction

Conclusions

References

Tables

Figures

◀

▶

◀

▶

Back

Close

Full Screen / Esc

Printer-friendly Version

Interactive Discussion



**Photoacoustic and  
nephelometric  
spectroscopy of  
aerosol properties**

N. Sharma et al.

Title Page

Abstract

Introduction

Conclusions

References

Tables

Figures

⏪

⏩

◀

▶

Back

Close

Full Screen / Esc

Printer-friendly Version

Interactive Discussion



atmosphere, while cooling the Earth's surface, thereby affecting convective processes and cloud properties and lifecycle. Some particles including most organics, sulphates, and salts scatter solar radiation efficiently without absorption, hence cooling the atmosphere (Chýlek et al., 1995) and reducing atmospheric visibility (Tang et al., 1981; Moosmüller and Arnott, 2009). These different aerosol species are released or formed into the atmosphere as a result of anthropogenic, biogenic, and other natural processes (like wind-driven dust entrainment) and significantly affect climate by means of their direct and indirect radiative forcing (Parry et al., 2007).

The efficiency of aerosols to absorb and scatter solar radiation depends upon particles characteristics like size, morphology, and refractive index. Therefore, aerosol absorption and scattering coefficients exhibit distinct wavelength dependencies. A number of experimental studies have been conducted to investigate the wavelength dependence of scattering and absorption of atmospheric aerosol exhibiting complex mixing of different components (e.g., Gyawali et al., 2012, 2013; Flowers et al., 2010; Bergstrom et al., 2007). Several controlled laboratory studies have also been performed, generating aerosols including soot, salt, and biomass burning particles and controlling or studying in detail the mixing state of different components (e.g., Sheridan et al., 2005; Lewis et al., 2008; Cross et al., 2010). Absorbing carbonaceous aerosols are termed light absorbing carbon and include soot and brown carbon (Bond and Bergstrom, 2006; Andreae and Gelencsér, 2006). An inverse dependence of the absorption coefficient on wavelength  $\lambda$  (i.e.,  $\lambda^{-1}$ ) has typically been observed for absorption by small soot particles (e.g., Bergstrom et al., 2002). In general, over a limited wavelength range, the absorption coefficient is approximately proportional to  $\lambda^{-b}$ . While for small soot particle  $b \sim 1$ , for brown carbon particles that can be generated for example from smoldering biomass burning, the value of the exponent  $b$  is wavelength dependent and is typically significantly greater than 1 for shorter visible and UV wavelengths leading to much enhanced absorption in the blue part of the solar spectrum (e.g., Sun et al., 2007; Lewis et al., 2008; Lack et al., 2012; Ramanathan et al., 2005). Salts, such as NaCl and  $(\text{NH}_4)_2\text{SO}_4$ , are non-absorbing in the visible and contribute to light extinction

mostly by scattering the incident radiation (Abu-Rahmah et al., 2006; Irshad et al., 2009; Chamailard et al., 2003; Schnaiter et al., 2006).

Measurement of the wavelength dependence of aerosol optical properties has been a challenging task, due to the dependence of optical properties on highly variable parameters such as mixing, morphology, composition, size and due to the inhomogeneous distribution of aerosols in the atmosphere. Integrating nephelometry is the most common technique for measuring in-situ aerosol scattering coefficients (Heintzenberg and Charlson, 1996; Abu-Rahmah et al., 2006). The two most common types of nephelometers are: (a) direct integrating nephelometer and (b) reciprocal integrating nephelometer (Marcos, 1999). A number of in-situ measurement techniques for the quantification of light absorption by aerosols have been available for years. The photoacoustic technique is currently gaining recognition due to its higher accuracy with respect to filter-based instruments and due to the availability of commercial instruments (Moosmüller et al., 2009; Lack et al., 2008). Several photoacoustic instrument designs have been developed by different groups for applications in the field of atmospheric measurements. Modern photoacoustic instruments typically exploit the high brightness and directionality of laser sources; however, these sources are generally monochromatic.

The commercially available photoacoustic spectrometer (PASS-3, by DMT Inc.), has evolved from its prototype single wavelength photoacoustic spectrometer (Arnott et al., 1999) and the dual wavelength photoacoustic spectrometer (Lewis et al., 2008) to the 3-wavelength instrument at 405, 532 and 781 nm, each wavelength being generated by an individual laser. These instruments also simultaneously measure aerosol scattering by reciprocal nephelometric technique. From the simultaneous measurement of the extensive absorption and scattering coefficients, provided by the integrated photoacoustic and nephelometer, one can obtain the aerosol single scattering albedo (SSA), which is the ratio of the scattering to the extinction coefficients. The SSA is an intensive quantity and is one of the fundamental parameters needed to calculate the aerosol radiative forcing (e.g., Chylek and Wong, 1995). The simultaneous measurement of absorption

## Photoacoustic and nephelometric spectroscopy of aerosol properties

N. Sharma et al.

Title Page

Abstract

Introduction

Conclusions

References

Tables

Figures



Back

Close

Full Screen / Esc

Printer-friendly Version

Interactive Discussion



## Photoacoustic and nephelometric spectroscopy of aerosol properties

N. Sharma et al.

Title Page

Abstract

Introduction

Conclusions

References

Tables

Figures



Back

Close

Full Screen / Esc

Printer-friendly Version

Interactive Discussion



and scattering coefficients with these instruments allows obtaining additional information from the same aerosol sample, in contrast to instruments which provide only an estimate of absorption, such as the aethalometer, the Particle Soot/Absorption Photometer (PSAP), and the Multi-Angle Absorption Photometer (MAAP).

A photoacoustic instrument discussed in Lack et al. (2006) uses a multi-pass cell to increase sensitivity at a single wavelength (532 nm). The latest multi-wavelength development of this instrument operates at three wavelengths: 404, 532, and 658 nm. Another multi-wavelength photoacoustic instrument developed by Ajtai et al. (2010) at the University of Szeged, Hungary measures the aerosol absorption simultaneously at four different wavelengths (266, 355, 532, and 1064 nm) by using a single laser source and higher harmonics generation. In a recent development, a tunable narrow linewidth Optical Parametrical Oscillator (OPO) has been combined with a photoacoustic cell for the sequential measurement of aerosol absorption coefficients over a wide spectral range (Haisch et al., 2012).

The main motivation behind the development of new instrumentation with increasing number of operating wavelengths is the role that wavelength dependencies of aerosol absorption and scattering have on radiative forcing and climate. The use of a broad-band laser source is an alternative to high power tunable lasers (such as the OPO) or the increased number of single wavelength sources in current photoacoustic spectrometers (as in the PASS-3). Supercontinuum, white light lasers are currently gaining great interest in biomedical applications, optical communications, as well as in fundamental spectroscopy due to their broad spectral bandwidth, high power, high stability, and relatively flat spectrum. Although supercontinuum generation has its roots in the pioneering work by Alfano and Shapiro in the early 1970's (Alfano and Shapiro, 1970), compact and robust supercontinuum lasers have become commercially available only in the last decade. Typically in these table-top systems, the supercontinuum generation is based on the spectral broadening of ultrashort laser pulses in photonic crystal fibers due to their high optical nonlinearity (Russell, 2003; Knight, 2003; Ranka et al., 2000; Dudley et al., 2006).





## Photoacoustic and nephelometric spectroscopy of aerosol properties

N. Sharma et al.

Title Page

Abstract

Introduction

Conclusions

References

Tables

Figures

◀

▶

◀

▶

Back

Close

Full Screen / Esc

Printer-friendly Version

Interactive Discussion

along their axis, and the laser beam propagates coaxial to the airflow. The sample flow is maintained at a rate of  $\sim 0.6$  lpm by using a critical orifice and a pump. The critical orifice also acoustically isolates the photoacoustic cell from the pump.

The photoacoustic cell consists of an acoustic resonator of length  $\sim 118$  mm which is approximately equal to half of the acoustic wavelength, and diameter 6.35 mm. The resonator is equipped with a hearing aid microphone (Knowles Inc. model# EK 23028) to measure the acoustic signal generated in the photoacoustic process (Tam, 1986). The optical power at the filter-selected wavelength band is modulated at the resonant acoustic frequency of the cell ( $\sim 1.5$  kHz) by using an optical chopper (New Focus model #3501). The modulated light enters the cell through a Brewster window. When sample particles absorb the modulated laser radiation, an acoustic signal is generated. The resonator amplifies the signal improving the signal to noise ratio. The microphone mounted in the resonator at the acoustic antinode detects the acoustic signal as a pressure change on its surface. The absorption coefficient of the aerosol is given by:

$$\beta_{\text{abs}} = \frac{P_m A_{\text{res}} \pi^2 f_0}{P_L (\gamma - 1) Q} \quad (1)$$

where,  $P_m$  is the pressure at the microphone at the resonant frequency  $f_0$ ,  $P_L$  is the laser power;  $A_{\text{res}}$  is the area of the geometric resonator cross section,  $\gamma$  is the ratio of specific heat at constant pressure and volume, and  $Q$  is the quality factor of the resonator (Rosencwaig, 1980; Arnott et al., 1999; Lewis et al., 2008; Moosmüller et al., 2009)  $\sim 20.9$  for our cell.

The scattering cell incorporates a reciprocal integrating nephelometer design (Marcos, 1999). The cell is equipped with two apertures of  $\sim 6.5$  mm diameter, and the scattering measurements are performed in the volume between these apertures. The apertures serve to decrease background radiation and to limit the truncation angle to  $\pm 5^\circ$ . The “scattering photodiode” (ThorLabs FDS100) used to detect the scattering signal is mounted on top of the nephelometer cell between the two apertures. A Lambertian diffuser is placed in front of the photodiode to provide an integrated cosine-weighted

**Photoacoustic and  
nephelometric  
spectroscopy of  
aerosol properties**

N. Sharma et al.

Title Page

Abstract

Introduction

Conclusions

References

Tables

Figures

⏪

⏩

◀

▶

Back

Close

Full Screen / Esc

Printer-friendly Version

Interactive Discussion



scattering signal. The laser radiation that propagates through the photoacoustic cell without being absorbed or scattered by the aerosols and gases within the cells, is detected by a photodiode (ThorLabs FDS100, we will refer to it as the “extinction photodiode”), mounted on an integrating sphere for measuring the total optical power entering it.

A control box incorporates an HEPA filter and a solenoid switch that the operator (or a computer digital signal) can periodically turn on to let the sample flow through an HEPA filter before reaching the measurement cell; this procedure is used to measure the background signal with particles removed from the sample. The control box also contains a sensor to measure the sample air pressure. The scattering and absorption background signals are due to electronic noise, molecular Rayleigh scattering, absorption by gases like  $\text{NO}_2$  present in the sampled air, and scattering or absorption of the laser beam at the windows and walls of the cells. In our experiments, background measurements were done for every minute of sample measurement. The background signal obtained for scattering and absorption were in the order of  $10^3$  and  $10^2 \text{ Mm}^{-1}$ , respectively. The background values of absorption and scattering are subtracted from the measured values to obtain the actual absorption and scattering by the aerosol particles alone. The outlet sample line from the photoacoustic has a temperature and RH sensor.

Instrument data are acquired with a National Instruments data acquisition card that has 8 channels for synchronous acquisition (NI PCI-6143) and a desktop PC. The card also provides a TTL signal to drive the chopper at the reference frequency and phase. LabView software includes functions of lock-in amplifier and Fast Fourier Transform (FFT) analyzer for phase sensitive detection of the photoacoustic signal and reduction of the noise in the microphone signal (Arnott et al., 1999; Scofield, 1994; Scott et al., 2001). The FFT is also used to measure the transmitted laser and scattered power.

During some of the experiments we simultaneously operated a commercial 3-wavelength photoacoustic/nephelometer spectrometer (PASS-3 by DMT Inc.) and a Scanning Mobility Particle Sizer (SMPS by TSI model# 3080). The PASS-3

simultaneously measures the aerosol scattering and absorption at 405, 532 and 781 nm, while our current instrument measures scattering and absorption at one wavelength at a time.

### 3 Aerosol generation and delivery system

Laboratory generated kerosene soot and nebulized salt (NaCl) aerosols were used to calibrate and test the instrument. Soot was generated with a simple kerosene lamp sold for domestic use. Salt in aqueous solution was nebulized using an ultrasonic mist maker or an aerosol generator (TSI 3076). The nebulized salt solution was then dried by passing it through a dessicator (anhydrous drierite) that reduced the sample RH value to  $\sim 30\%$  before delivery to the instrument. The aerosol sample was forced through the sample line by an eductor pump which provided diluted, relatively steady aerosol concentrations.

Because our instrument operated only at one wavelength-band at a time, in order to compare the aerosol optical properties obtained at each wavelength-band the aerosol concentration needed to vary slowly and monotonically and the size distribution needed to change as little as possible. This was achieved by using an iron lung, which is basically a conducting bag lined inside a drum filled with the aerosol (Arnold et al., 2013). As the aerosol is drawn from the lung by the instruments, the bag gradually collapses resulting in a slow and monotonically decaying particle concentration with small variations in the size distribution. The typical absorption and scattering coefficients measured by the SC-PNS and PASS-3 at the iron lung output were in the order of  $2000\text{--}3000\text{ M m}^{-1}$ . The SMPS was used for monitoring the size distribution and concentration of the aerosol sample delivered from the iron lung. The average mode number diameter (MND) and geometric standard deviation (GSD) for soot were  $208(\pm 16)\text{ nm}$  and  $1.77(\pm 0.03)$ , respectively over a period of 2 h and 6 min. For salt, the average MND and the GSD measured by SMPS were  $140(\pm 7)\text{ nm}$  and  $1.77(\pm 0.012)$ , respectively

## Photoacoustic and nephelometric spectroscopy of aerosol properties

N. Sharma et al.

Title Page

Abstract

Introduction

Conclusions

References

Tables

Figures

◀

▶

◀

▶

Back

Close

Full Screen / Esc

Printer-friendly Version

Interactive Discussion



over a period of 2 h and 6 min. The number in parenthesis represents one standard deviation (Fig. 4).

#### 4 Instrument calibration

The calibration procedure of the SC-PNS involves four steps: (1) calibration of the extinction photodiode, (2) measurement of the resonance response of the acoustic cell, (3) calibration of the scattering photodiode (including the diffuser angular response), and (4) absorption calibration (calibration of the microphone response).

The extinction photodiode is calibrated by comparing the output signal of the photodiode with the power of the laser at the different wavelength bands as measured by a calibrated power meter (ThorLabs, PM100-D) at the end of SC-PNS cells.

The resonance response of the acoustic cell is measured using a piezoelectric transducer by scanning its emission frequency and recording the signal at the microphone. The microphone signal is then compared to a Lorentzian resonance curve and a least square fit is performed using a second order polynomial to obtain the values of the resonator quality factor,  $Q$  and the resonance frequency,  $f_0$  (Arnott et al., 1999).

The absorption and scattering calibration procedure for the SC-PNS is based on the measurement of the single-pass light extinction. High sample concentrations yielding absorption or scattering coefficients up to 40 000–60 000  $\text{Mm}^{-1}$  are necessary to obtain a significant extinction signals in the order of 1–3 % (Eq. 3) due to the short optical path  $L$  within the cell (405 mm). The scattering calibrations at the different wavelengths, are carried out using non-absorbing aerosols (e.g., salt) while absorbing aerosols (e.g., soot) are used for absorption calibrations. The calibration coefficients are determined by comparing the scattering and absorption signals to the extinction signal and exploiting the optical closure relation given by:

$$\beta_{\text{ext}} = \beta_{\text{sca}} + \beta_{\text{abs}} \quad (2)$$

where  $\beta_{\text{ext}}$  is the extinction coefficient calculated from the equation:

## Photoacoustic and nephelometric spectroscopy of aerosol properties

N. Sharma et al.

Title Page

Abstract

Introduction

Conclusions

References

Tables

Figures



Back

Close

Full Screen / Esc

Printer-friendly Version

Interactive Discussion





wavelength-dependence in the calibration variability and that the instrument response is quite linear over large scattering and absorption ranges.

## 5 Results and discussion

After calibration, the SC-PNS was tested with kerosene soot and nebulized NaCl salt in two separate experiments and the results were compared to the PASS-3 data. As mentioned earlier, the PASS-3 operated continuously during the experiment measuring at three wavelengths simultaneously, while the SC-PAS was operated in sequence, one wavelength at a time; measurements were done with each optical filter for  $\sim 1$  min. In the following discussion, we will refer to “run” as a full set of the different optical filters (from 1 to 5). We performed background measurements before and after sample measurement on each filter. Measurements continued until the particle concentration dropped to a value too low to provide a reasonable signal to noise ratio on the SC-PNS. The experiment for each aerosol type lasted for about 2 h with 5–6 complete runs. A comparison of the data obtained from the two instruments is discussed next.

The PASS-3 and the SC-PNS data were first normalized to the average of the PASS-3 signal over the time correspondent to each wavelength of the first run. This was done to normalize for the changes in aerosol concentration over the span of the entire experiment and to allow for a direct comparison of the different SC-PAS wavelengths.

The two instruments operate at different wavelengths and different bandwidths; therefore, in order to compare the measurements, the absorption and scattering measured by the PASS-3 was interpolated over the spectrum of the supercontinuum through each filter. The interpolation for the wavelengths correspondent to the filters F1 and F2 was done using the Ångström exponent for absorption and scattering calculated from the 405 and 532 nm wavelengths from the PASS-3 using Eq. (4). The interpolation for the wavelengths correspondent to the filters F3, F4 and F5 was done using the Ångström exponents calculated from the 532 and 781 nm data from the PASS-3.

$$\beta_{\text{abs(sca)}}(\lambda) = C \cdot \lambda^{-\alpha_{\text{abs(sca)}}}, \quad (4)$$

### Photoacoustic and nephelometric spectroscopy of aerosol properties

N. Sharma et al.

Title Page

Abstract

Introduction

Conclusions

References

Tables

Figures

⏪

⏩

◀

▶

Back

Close

Full Screen / Esc

Printer-friendly Version

Interactive Discussion





## 5.1 Kerosene soot

Figure 6a shows the absorption coefficient as a function of wavelength with a power law fit of the SC-PNS data yielding an Absorption Ångström Exponent (AAE) of  $\sim 0.972$  ( $\pm 0.001$ ). This value is consistent with the  $\lambda^{-1}$  dependence demonstrated in a number of theoretical and experimental studies previously conducted on kerosene soot (Sheridan et al., 2005; Bergstrom et al., 2002; Moosmüller and Arnott, 2009). During the Reno aerosol optics study (Sheridan et al., 2005) the AAE for kerosene soot was measured to be in the range of 0.94 to 1.0. The Scattering Ångström Exponent (SAE) in our experiment is  $\sim 1.611$  ( $\pm 0.005$ ) as shown in Fig. 6b. For comparison, Gyawali et al. (2012) obtained a SAE of 1.88 for kerosene soot; we point out that the SAE is strongly dependent on particle size. The single scattering albedo as a function of wavelength is shown in Fig. 6c and is decreasing with increasing wavelength above 550 nm for both instruments. Measurements from the two instruments agree with each other within the statistical uncertainties of the data.

## 5.2 Salt

Common salt (NaCl) aerosol is white ( $SSA = 1$ ) and is expected to show negligible absorption at visible wavelengths. Figure 7a shows the absorption coefficient of salt obtained from SC-PNS and PASS-3. The absorption coefficients from the two instruments are zero within their respective errors demonstrating, as expected, that scattering does not interfere with the absorption measurement, or in other words, the photoacoustic effect is insensitive to scattering. On the other hand, the values of scattering coefficients obtained from the two instruments show strong wavelength dependence (Fig. 7b). In view of the zero absorption, the single scattering albedo (Fig. 7c) had a constant value  $\sim 1$ , irrespective of wavelength.

## Photoacoustic and nephelometric spectroscopy of aerosol properties

N. Sharma et al.

Title Page

Abstract

Introduction

Conclusions

References

Tables

Figures

◀

▶

◀

▶

Back

Close

Full Screen / Esc

Printer-friendly Version

Interactive Discussion

### 5.3 Nitrogen dioxide

Nitrogen dioxide absorbs throughout the visible region and therefore can be used to evaluate the absorption measured by the instrument of the SC-PNS. With this aim, we conducted an experiment by maintaining a continuous flow of 101.3 ( $\pm 2$ ) ppm (mole %)  $\text{NO}_2$  in air through the instrument. The difference between the scattering coefficient of particle free air and the  $\text{NO}_2$  mixture is negligible in the visible region, and therefore the measured extinction coefficient of the laser radiation should correspond to the absorption coefficient. The photoacoustic signal (expressed in units inverse megameters as calibrated with kerosene soot) and the scattering coefficient were measured directly and the extinction coefficient was calculated from the laser powers measured with the extinction photodiode at the integrating sphere using Eq. (6).

$$\beta_{\text{ext}} = \left( \frac{-1}{L} \right) \ln \left( \frac{I}{I_0} \right) \quad (6)$$

where  $I_0$  is the laser intensity measured while particle-free dry air was flowing through the instrument,  $I$  is the laser intensity measured with the 101.3 ppm  $\text{NO}_2$  mixture flowing in the cell, and  $L$  is the cell length.

The photoacoustic signal and the extinction coefficient obtained by our instrument at each wavelength band were compared to the absorption coefficients calculated from the  $\text{NO}_2$  absorption cross sections using the HITRAN database at 294 K (Orphal and Chance, 2003; Rothman et al., 2003). Figure 8a shows a plot of the photoacoustic signal and extinction coefficient measured by our instrument and that calculated from the HITRAN database as a function of wavelength and Fig. 8b shows a plot of the photoacoustic signal and extinction coefficient measured as a function of the absorption coefficient from the HITRAN database for an  $\text{NO}_2$  concentration of 101.3 ppm. For a direct comparison, the absorption coefficient from the HITRAN database was weighted by the spectral radiance at each wavelength and integrated over the complete wavelength band of each filter to obtain the absorption coefficient for the corresponding filter.

Title Page

Abstract

Introduction

Conclusions

References

Tables

Figures

⏪

⏩

◀

▶

Back

Close

Full Screen / Esc

Printer-friendly Version

Interactive Discussion



**Photoacoustic and nephelometric spectroscopy of aerosol properties**

N. Sharma et al.

Title Page

Abstract

Introduction

Conclusions

References

Tables

Figures

⏪

⏩

◀

▶

Back

Close

Full Screen / Esc

Printer-friendly Version

Interactive Discussion

Absorption by  $\text{NO}_2$  decreases rapidly with increasing wavelengths while is accompanied by photodissociation at UV and blue wavelengths ( $\sim 289\text{--}422\text{ nm}$ ). The quantum yield of photodissociation for  $\text{NO}_2$  is approximately 1 up to 370 nm and then decreases rapidly reaching a value of 0.02 around 422 nm (Seinfeld and Pandis, 1998). Filter 1 ( $417 \pm 60\text{ nm}$ ) has a bandwidth range from 386 to 456 nm which overlaps with the expected photodissociation range. Therefore, as expected, for filter 1 we measured a photoacoustic signal ( $\beta_{\text{abs}} \text{ PAS}$ ) lower than the calculated  $\text{NO}_2$  absorption coefficient and the measured extinction coefficient (Tian et al., 2013). We corrected for the photodissociation effect by weighting the quantum yield by the spectral radiance of filter 1 ( $\varphi_{\text{net}}$ ) and dividing the photoacoustic signal by  $(1 - \varphi_{\text{net}})$ . The corrected  $\beta_{\text{abs}}$  (represented in the graph by the hollow circle in Fig. 8b) is increased by a factor of  $\sim 1.3$ . No correction is needed for the other wavelength bands due to the negligible photodissociation quantum yield at these wavelengths. The extinction and the absorption coefficients (including the corrected value for filter 1) lie on the 1 : 1 line ( $\beta_{\text{abs}} \text{ PAS}$  and  $\beta_{\text{ext}} \text{ PAS} : \beta_{\text{abs}} \text{ HITRAN}$ ) within the error limits. The uncertainty in the absorption coefficient calculated from the HITRAN database is calculated as the square root of the sum of squares of 2 % uncertainty in  $\text{NO}_2$  concentration, as per gas specification, and 2 % uncertainty in  $\text{NO}_2$  absorption cross section indicated in Orphal and Chance (2003). From our analysis and plot we omitted the absorption coefficient for the filter centered at 675 nm (filter 5), which was  $\sim 1000 \text{ Mm}^{-1}$  because  $\text{NO}_2$  absorption cross sections beyond 663 nm are not available in the HITRAN database that we used.

The results of this experiment demonstrate the validity of the absorption calibration procedure discussed earlier, and indirectly also the scattering calibration, as the absorption calibration with kerosene soot is based on the difference between extinction and calibrated scattering, as previously suggested by Arnott et al. (2000).

## 6 Instrumental noise and minimum detection limits versus integration time

The instrumental noise and drifts were studied by operating the instrument with aerosol-free air (using indoor air filtered with a HEPA filter) for each wavelength band. The instrument stability and the minimum detection limit of the instrument were analyzed using Allan deviation plots. The instrument is considered to be stable for a length of time when the signal is free from drifts. Averaging the signal over this time reduces the noise of the instrument, improves the signal to noise ratio and hence the minimum detection limit of the instrument. For a signal which includes random noise and instrumental drift, the Allan deviation firstly decreases proportionally with the reciprocal of the square root of the averaging (integration) time and then increases as instrumental drift becomes significant (Werle et al., 1993; Skřínský et al., 2009).

We used a Matlab code written by Fabian Czerwinski (Czerwinski, 2010) to calculate the Allan deviation for the absorption and scattering signals for the SC-PNS and the PASS-3 as shown in Fig. 9a and b, respectively. The lowest point in each plot indicates the minimum detectable absorption and scattering coefficients at the respective wavelength and averaging time. Table 2 lists the approximate values of minimum detectable absorption and scattering coefficients obtained at each wavelength band of the SC-PNS for an equal integration time of 60 s. For comparison we also added the minimum detection limits at 60 s integration time similarly calculated for the PASS-3.

Minimum detectable absorption of  $0.5$ ,  $2$  and  $1 \text{ Mm}^{-1}$  and minimum detectable scattering of less than  $2 \text{ Mm}^{-1}$  can be achieved for  $542$ ,  $607$  and  $675 \text{ nm}$  wavelengths by integrating the signal for  $\sim 60 \text{ s}$ . These values of minimum detectable absorption and scattering makes the instrument capable of measuring ambient aerosols even in environments with medium-low aerosol concentrations.

## AMTD

6, 6293–6327, 2013

### Photoacoustic and nephelometric spectroscopy of aerosol properties

N. Sharma et al.

Title Page

Abstract

Introduction

Conclusions

References

Tables

Figures

⏪

⏩

◀

▶

Back

Close

Full Screen / Esc

Printer-friendly Version

Interactive Discussion

## 7 Conclusions

We developed a new photoacoustic-nephelometer instrument using a supercontinuum laser as light source for the measurement of absorption and scattering coefficients of aerosol samples at multiple wavelengths (i.e., 417, 475, 542, 607, and 675 nm).

5 The instrument was tested with kerosene soot and common salt for the wavelength dependence of aerosol optical properties and the results obtained were compared to a simultaneously operating commercial 3-wavelength photoacoustic and nephelometer instrument (PASS-3). The value of absorption and scattering Ångström exponent obtained for soot from our instrument agreed closely with values available in literature.

10 Salt being a white aerosol, showed negligible absorption at visible wavelengths demonstrating the lack of scattering interferences on the absorption measurements, in contrast to filter-based measurements. Scattering coefficients of salt aerosol as obtained by our instrument, showed strong wavelength dependence departing from a simple power law. The absorption and scattering coefficients obtained with the commercial instrument and interpolated on the supercontinuum wavelength bands agreed with the observations from the SC-PNS. The absorption coefficient as measured for the first four wavelength bands agree well with theoretical calculations when measuring a mixture of NO<sub>2</sub> in air. As the instrument operates over broad wavelength bands the knowledge of the spectral details of absorption by gaseous species is less critical that for single  
20 line laser-based photoacoustic systems.

The current version of the instrument measures at each wavelength band, one at a time, which requires a stable size distribution and monotonic (or at least well-constrained) variation in the concentration of the sample particles, to measure accurate aerosol absorption and scattering spectra. Efforts toward the development of a field deployable instrument are currently under way by improving the current instrument to measure simultaneously at different wavelengths and to expand the measurement spectral region to the NIR to allow the characterization of aerosol optical properties over  
25 most of the solar spectrum. Due to the minimum detectable absorption and scattering

## Photoacoustic and nephelometric spectroscopy of aerosol properties

N. Sharma et al.

Title Page

Abstract

Introduction

Conclusions

References

Tables

Figures



Back

Close

Full Screen / Esc

Printer-friendly Version

Interactive Discussion



coefficients, the instrument can find applications in laboratory as well as in field studies down to medium-low pollution environmental conditions. The instrument can provide valuable and unique information on the wavelength dependence of the optical properties of ambient and laboratory-generated aerosols.

- 5 *Acknowledgements.* This material is based upon work supported by the National Science Foundation under Grant No. AGS-1040046, by NASA EPSCoR under Cooperative Agreement No. NNX10AR89A, by NASA ROSES under Grant No. NNX11AB79G, by Michigan Tech start-up fund and by a Michigan Tech Research Excellence Fund-Research Seed Grant.

## References

- 10 Abu-Rahmah, A., Arnott, W. P., and Moosmüller, H.: Integrating nephelometer with a low truncation angle and an extended calibration scheme, *Meas. Sci. Technol.*, 17, 1723–1732, doi:10.1088/0957-0233/17/7/010, 2006.
- Ajtai, T., Filep, Á., Schnaiter, M., Linke, C., Vragel, M., Bozóki, Z., Szabó, G., and Leisner, T.: A novel multi-wavelength photoacoustic spectrometer for the measurement of the UV–vis–NIR spectral absorption coefficient of atmospheric aerosols, *J. Aerosol Sci.*, 41, 1020–1029, 15 2010.
- Alfano, R. and Shapiro, S.: Observation of self-phase modulation and small-scale filaments in crystals and glasses, *Phys. Rev. Lett.*, 24, 592, 1970.
- Andreae, M. O. and Gelencsér, A.: Black carbon or brown carbon? The nature of light-absorbing carbonaceous aerosols, *Atmos. Chem. Phys.*, 6, 3131–3148, doi:10.5194/acp-6-3131-2006, 20 2006.
- Arnold, I. J., Berger, C., Moosmüller, H., Sharma, N., and Mazzoleni, C.: The Iron Lung: A Device for the Continuous Delivery of Fine Particulate Matter *Rev. Sci. Instrum.*, submitted, 2013.
- 25 Arnott, W. P., Moosmüller, H., Rogers, C. F., Jin, T. F., and Bruch, R.: Photoacoustic spectrometer for measuring light absorption by aerosol: instrument description, *Atmos. Environ.*, 33, 2845–2852, 1999.

## Photoacoustic and nephelometric spectroscopy of aerosol properties

N. Sharma et al.

Title Page

Abstract

Introduction

Conclusions

References

Tables

Figures

⏪

⏩

◀

▶

Back

Close

Full Screen / Esc

Printer-friendly Version

Interactive Discussion



## Photoacoustic and nephelometric spectroscopy of aerosol properties

N. Sharma et al.

Title Page

Abstract

Introduction

Conclusions

References

Tables

Figures

◀

▶

◀

▶

Back

Close

Full Screen / Esc

Printer-friendly Version

Interactive Discussion



- Arnott, W. P., Moosmüller, H., and Walker, J. W.: Nitrogen dioxide and kerosene-flame soot calibration of photoacoustic instruments for measurement of light absorption by aerosols, *Rev. Sci. Instrum.*, 71, 4545–4552, doi:10.1063/1.1322585, 2000.
- Bergstrom, R. W., Russell, P. B., and Hignett, P.: Wavelength dependence of the absorption of black carbon particles: predictions and results from the TARFOX experiment and implications for the aerosol single scattering albedo, *J. Atmos. Sci.*, 59, 567–577, 2002.
- Bergstrom, R. W., Pilewskie, P., Russell, P. B., Redemann, J., Bond, T. C., Quinn, P. K., and Sierau, B.: Spectral absorption properties of atmospheric aerosols, *Atmos. Chem. Phys.*, 7, 5937–5943, doi:10.5194/acp-7-5937-2007, 2007.
- Bond, T. C. and Bergstrom, R. W.: Light absorption by carbonaceous particles: an investigative review, *Aerosol Sci. Tech.*, 40, 27–67, 2006.
- Chamaillard, K., Jennings, S., Kleefeld, C., Ceburnis, D., and Yoon, Y.: Light backscattering and scattering by nonspherical sea-salt aerosols, *J. Quant. Spectrosc. Ra.*, 79, 577–597, 2003.
- Chen, Y. and Bond, T. C.: Light absorption by organic carbon from wood combustion, *Atmos. Chem. Phys.*, 10, 1773–1787, doi:10.5194/acp-10-1773-2010, 2010.
- Chylek, P. and Wong, J.: Effect of absorbing aerosols on global radiation budget, *Geophys. Res. Lett.*, 22, 929–931, 1995.
- Chýlek, P., Videen, G., Ngo, D., Pinnick, R. G., and Klett, J. D.: Effect of black carbon on the optical properties and climate forcing of sulfate aerosols, *J. Geophys. Res.*, 100, 16325–16332, doi:10.1029/95jd01465, 1995.
- Cross, E. S., Onasch, T. B., Ahern, A., Wrobel, W., Slowik, J. G., Olfert, J., Lack, D. A., Massoli, P., Cappa, C. D., and Schwarz, J. P.: Soot particle studies – instrument inter-comparison – project overview, *Aerosol Sci. Tech.*, 44, 592–611, 2010.
- Czerwinski, F.: Allan v3.0 MATLABCentral, available at: <http://www.mathworks.com/matlabcentral/fileexchange/26659-allan-v3-0> (last access: 17 December 2012), 2010.
- Dudley, J. M., Genty, G., and Coen, S.: Supercontinuum generation in photonic crystal fiber, *Rev. Mod. Phys.*, 78, 1135, doi:10.1103/RevModPhys.78.1135, 2006.
- Flowers, B. A., Dubey, M. K., Mazzoleni, C., Stone, E. A., Schauer, J. J., Kim, S.-W., and Yoon, S. C.: Optical-chemical-microphysical relationships and closure studies for mixed carbonaceous aerosols observed at Jeju Island; 3-laser photoacoustic spectrometer, particle sizing, and filter analysis, *Atmos. Chem. Phys.*, 10, 10387–10398, doi:10.5194/acp-10-10387-2010, 2010.

**Photoacoustic and nephelometric spectroscopy of aerosol properties**

N. Sharma et al.

Title Page

Abstract

Introduction

Conclusions

References

Tables

Figures

◀

▶

◀

▶

Back

Close

Full Screen / Esc

Printer-friendly Version

Interactive Discussion



- Gyawali, M., Arnott, W. P., Zaveri, R. A., Song, C., Moosmüller, H., Liu, L., Mishchenko, M. I., Chen, L.-W. A., Green, M. C., Watson, J. G., and Chow, J. C.: Photoacoustic optical properties at UV, VIS, and near IR wavelengths for laboratory generated and winter time ambient urban aerosols, *Atmos. Chem. Phys.*, 12, 2587–2601, doi:10.5194/acp-12-2587-2012, 2012.
- 5 Gyawali, M., Arnott, W. P., Zaveri, R. A., Song, C., Pekour, M., Flowers, B., Dubey, M. K., Setyan, A., Zhang, Q., Harworth, J. W., Radney, J. G., Atkinson, D. B., China, S., Mazzoleni, C., Gorkowski, K., Subramanian, R., Jobson, B. T., and Moosmüller, H.: Evolution of multispectral aerosol optical properties in a biogenically-influenced urban environment during the CARES campaign, *Atmos. Chem. Phys. Discuss.*, 13, 7113–7150, doi:10.5194/acpd-13-7113-2013, 2013.
- 10 Haisch, C., Menzenbach, P., Bladt, H., and Niessner, R. R.: A wide spectral range photoacoustic aerosol absorption spectrometer, *Anal. Chem.*, 84, 8941–8945, doi:10.1021/ac302194u, 2012.
- Heintzenberg, J. and Charlson, R. J.: Design and applications of the integrating nephelometer: a review, *J. Atmos. Ocean. Tech.*, 13, 987–1000, 1996.
- 15 Horvath, H.: Atmospheric light absorption – a review, *Atmos. Environ. A-Gen.*, 27, 293–317, 1993.
- Irshad, R., Grainger, R. G., Peters, D. M., McPheat, R. A., Smith, K. M., and Thomas, G.: Laboratory measurements of the optical properties of sea salt aerosol, *Atmos. Chem. Phys.*, 9, 221–230, doi:10.5194/acp-9-221-2009, 2009.
- 20 Knight, J. C.: Photonic crystal fibres, *Nature*, 424, 847–851, 2003.
- Lack, D. A., Lovejoy, E. R., Baynard, T., Pettersson, A., and Ravishankara, A. R.: Aerosol absorption measurement using photoacoustic spectroscopy: sensitivity, calibration, and uncertainty developments, *Aerosol Sci. Tech.*, 40, 697–708, doi:10.1080/02786820600803917, 2006.
- 25 Lack, D. A., Cappa, C. D., Covert, D. S., Baynard, T., Massoli, P., Sierau, B., Bates, T. S., Quinn, P. K., Lovejoy, E. R., and Ravishankara, A.: Bias in filter-based aerosol light absorption measurements due to organic aerosol loading: evidence from ambient measurements, *Aerosol Sci. Tech.*, 42, 1033–1041, 2008.
- 30 Lack, D. A., Langridge, J. M., Bahreini, R., Cappa, C. D., Middlebrook, A. M., and Schwarz, J. P.: Brown carbon and internal mixing in biomass burning particles, *P. Natl. Acad. Sci. USA*, 109, 14802–14807, 2012.

## Photoacoustic and nephelometric spectroscopy of aerosol properties

N. Sharma et al.

Title Page

Abstract

Introduction

Conclusions

References

Tables

Figures

◀

▶

◀

▶

Back

Close

Full Screen / Esc

Printer-friendly Version

Interactive Discussion



- Lewis, K., Arnott, W. P., Moosmüller, H., and Wold, C. E.: Strong spectral variation of biomass smoke light absorption and single scattering albedo observed with a novel dual-wavelength photoacoustic instrument, *J. Geophys. Res.-Atmos.*, 113, D16203, doi:10.1029/2007jd009699, 2008.
- 5 Marcos, A.: Deriving the basic cell-reciprocal integrating nephelometer equation and its use for calibration purposes: a comprehensive approach, *Meas. Sci. Technol.*, 10, R1–R15, 1999.
- Moosmüller, H., and Arnott, W. P.: Particle optics in the Rayleigh regime, *JAPCA, J. Air Waste Manage.*, 59, 1028–1031, doi:10.3155/1047-3289.59.9.1028, 2009.
- Moosmüller, H., Chakrabarty, R. K., and Arnott, W. P.: Aerosol light absorption and its measurement: a review, *J. Quant. Spectrosc. Ra.*, 110, 844–878, doi:10.1016/j.jqsrt.2009.02.035, 10 2009.
- Moosmüller, H., Chakrabarty, R. K., Ehlers, K. M., and Arnott, W. P.: Absorption Ångström coefficient, brown carbon, and aerosols: basic concepts, bulk matter, and spherical particles, *Atmos. Chem. Phys.*, 11, 1217–1225, doi:10.5194/acp-11-1217-2011, 2011.
- 15 Moosmüller, H., Engelbrecht, J. P., Skiba, M., Frey, G., Chakrabarty, R. K., and Arnott, W. P.: Single scattering albedo of fine mineral dust aerosols controlled by iron concentration, *J. Geophys. Res.*, 117, D11210, doi:10.1029/2011jd016909, 2012.
- Orphal, J. and Chance, K.: Ultraviolet and visible absorption cross-sections for HITRAN, *J. Quant. Spectrosc. Ra.*, 82, 491–504, 2003.
- 20 Ramanathan, V., Chung, C., Kim, D., Bettge, T., Buja, L., Kiehl, J., Washington, W., Fu, Q., Sikka, D., and Wild, M.: Atmospheric brown clouds: impacts on South Asian climate and hydrological cycle, *P. Natl. Acad. Sci. USA*, 102, 5326–5333, 2005.
- Ranka, J. K., Windeler, R. S., and Stentz, A. J.: Visible continuum generation in air-silica microstructure optical fibers with anomalous dispersion at 800 nm, *Opt. Lett.*, 25, 25–27, 2000.
- 25 Rosencwaig, A.: *Photoacoustics and Photoacoustic Spectroscopy*, Wiley, New York, NY, 1980.
- Rothman, L., Barbe, A., Chris Benner, D., Brown, L., Camy-Peyret, C., Carleer, M., Chance, K., Clerbaux, C., Dana, V., and Devi, V. M.: The HITRAN molecular spectroscopic database: edition of 2000 including updates through 2001, *J. Quant. Spectrosc. Ra.*, 82, 5–44, 2003.
- 30 Roy, A., Leproux, P., Roy, P., Auguste, J.-L., and Couderc, V.: Supercontinuum generation in a nonlinear Yb-doped, double-clad, microstructured fiber, *J. Opt. Soc. Am. B*, 24, 788–791, 2007.
- Russell, P.: *Photonic Crystal Fibers*, Science, 299, 358–362, 2003.

**Photoacoustic and nephelometric spectroscopy of aerosol properties**

N. Sharma et al.

Title Page

Abstract

Introduction

Conclusions

References

Tables

Figures

◀

▶

◀

▶

Back

Close

Full Screen / Esc

Printer-friendly Version

Interactive Discussion



Schnaiter, M., Gimmler, M., Llamas, I., Linke, C., Jäger, C., and Mutschke, H.: Strong spectral dependence of light absorption by organic carbon particles formed by propane combustion, *Atmos. Chem. Phys.*, 6, 2981–2990, doi:10.5194/acp-6-2981-2006, 2006.

5 Scofield, J. H.: Frequency-domain description of a lock-in amplifier, *Am. J. Phys.*, 62, 129–132, 1994.

Scott, R. P., Langrock, C., and Kolner, B. H.: High-dynamic-range laser amplitude and phase noise measurement techniques, *IEEE J. Sel. Top. Quant.*, 7, 641–655, doi:10.1109/2944.974236, 2001.

10 Sheridan, P. J., Arnott, W. P., Ogren, J. A., Andrews, E., Atkinson, D. B., Covert, D. S., Moosmüller, H., Petzold, A., Schmid, B., Strawa, A. W., Varma, R., and Virkkula, A.: The Reno aerosol optics study: an evaluation of aerosol absorption measurement methods, *Aerosol Sci. Tech.*, 39, 1–16, doi:10.1080/027868290901891, 2005.

15 Skřínský, J., Janečková, R., Grigorová, E., Střížík, M., Kubát, P., Herecová, L., Nevrlý, V., Zelinger, Z., and Civiš, S.: Allan variance for optimal signal averaging – monitoring by diode-laser and CO<sub>2</sub> laser photo-acoustic spectroscopy, *J. Mol. Spectrosc.*, 256, 99–101, 2009.

Sun, H., Biedermann, L., and Bond, T. C.: Color of brown carbon: a model for ultraviolet and visible light absorption by organic carbon aerosol, *Geophys. Res. Lett.*, 34, L17813, doi:10.1029/2007GL029797, 2007.

20 Tam, A. C.: Applications of photoacoustic sensing techniques, *Rev. Mod. Phys.*, 58, 381–431, 1986.

Tang, I. N., Wong, W. T., and Munkelwitz, H. R.: The relative importance of atmospheric sulfates and nitrates in visibility reduction, *Atmos. Environ.*, 15, 2463–2471, doi:10.1016/0004-6981(81)90062-7, 1981.

25 Tian, G., Moosmüller, H., and Arnott, W. P.: Influence of photolysis on multispectral photoacoustic measurement of nitrogen dioxide concentration, *J. Air Waste Manage.*, 2013.

Werle, P., Mücke, R., and Slemr, F.: The limits of signal averaging in atmospheric trace-gas monitoring by tunable diode-laser absorption spectroscopy (TDLAS), *Appl. Phys. B*, 57, 131–139, 1993.

## Photoacoustic and nephelometric spectroscopy of aerosol properties

N. Sharma et al.

Title Page

Abstract

Introduction

Conclusions

References

Tables

Figures

⏪

⏩

◀

▶

Back

Close

Full Screen / Esc

Printer-friendly Version

Interactive Discussion

**Table 1.** Optical specifications of single-band bandpass filters used in the supercontinuum integrated photoacoustic-nephelometer spectrometer.

Filter identifier	Center wavelength [nm]	Transmission band [nm]	FWHM bandwidth [nm]	Average transmittance [%]	Resulting laser power [mW]
F1	417	387–447	64.2	> 90	15.6
F2	475	450–500	56.4	> 90	26.5
F3	542	517–567	56.8	> 93	45.6
F4	607	572–642	80	> 92	86.4
F5	675	641.5–708.5	73.7	> 90	64.4

## Photoacoustic and nephelometric spectroscopy of aerosol properties

N. Sharma et al.

**Table 2.** Minimum detectable absorption (MDA) and scattering (MDS) coefficients for 60 s integration time.

SC-PNS Center wavelength [nm]	MDA [ $\text{M m}^{-1}$ ]	MDS [ $\text{M m}^{-1}$ ]	Laser power [mW]	PASS-3 wavelength [nm]	MDA [ $\text{M m}^{-1}$ ]	MDS [ $\text{M m}^{-1}$ ]	Laser power [mW]
417	4	21	15.6	405	0.4	0.2	254
475	3	6	26.5	–	–	–	–
542	0.5	1.5	45.6	532	8	1.7	89
607	2	1	86.4	–	–	–	–
675	1	0.5	64.4	–	–	–	–
–	–	–	–	781	0.3	0.8	501

Title Page

Abstract

Introduction

Conclusions

References

Tables

Figures

⏪

⏩

◀

▶

Back

Close

Full Screen / Esc

Printer-friendly Version

Interactive Discussion

**Photoacoustic and nephelometric spectroscopy of aerosol properties**

N. Sharma et al.

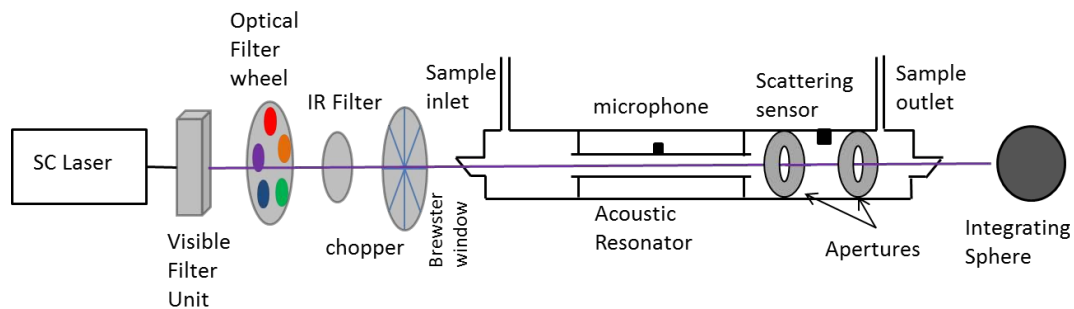


**Fig. 1.** Schematics of the supercontinuum integrated photoacoustic-nephelometer spectrometer.

[Title Page](#)[Abstract](#)[Introduction](#)[Conclusions](#)[References](#)[Tables](#)[Figures](#)[⏪](#)[⏩](#)[◀](#)[▶](#)[Back](#)[Close](#)[Full Screen / Esc](#)[Printer-friendly Version](#)[Interactive Discussion](#)

**Photoacoustic and  
nephelometric  
spectroscopy of  
aerosol properties**

N. Sharma et al.

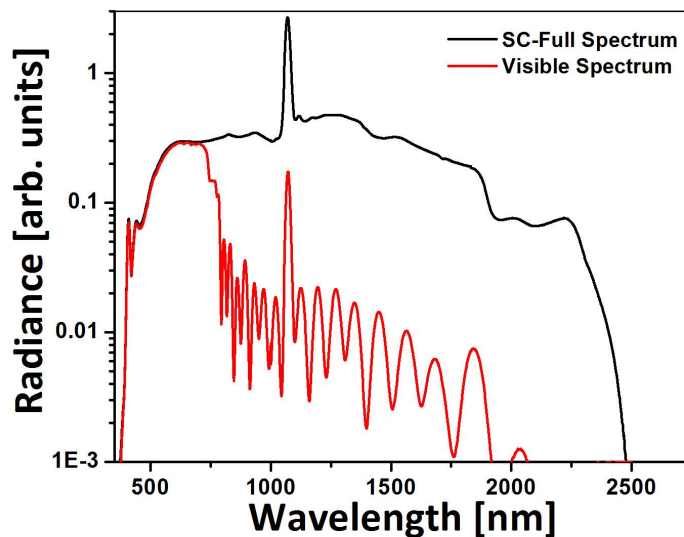


**Fig. 2.** Supercontinuum full spectrum and spectrum with visible filter unit.

Title Page

Abstract

Introduction

Conclusions

References

Tables

Figures

◀

▶

◀

▶

Back

Close

Full Screen / Esc

Printer-friendly Version

Interactive Discussion

Photoacoustic and  
nephelometric  
spectroscopy of  
aerosol properties

N. Sharma et al.

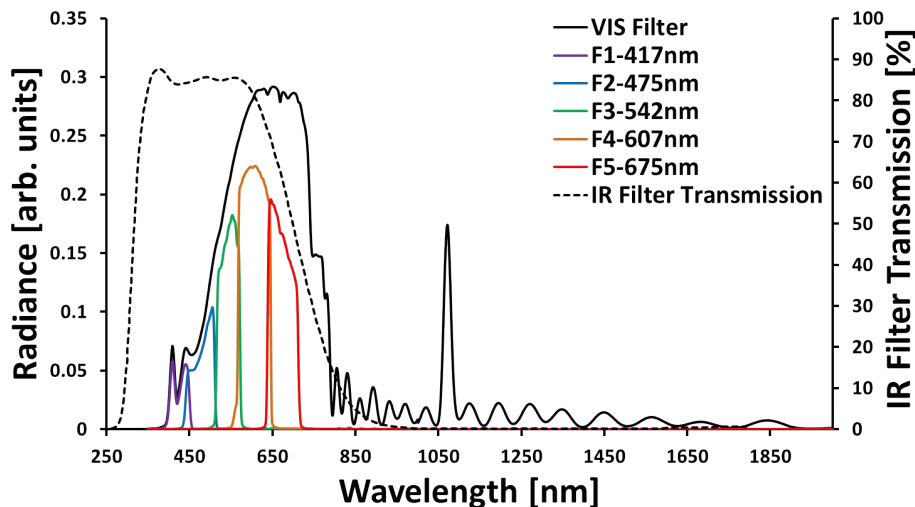


**Fig. 3.** Radiance spectra from single band filters (colored lines). Longer wavelengths are filtered out by using an infrared blocking filter (dashed line represents the transmission spectrum of the IR filter on the right vertical axis).

Title Page

Abstract

Introduction

Conclusions

References

Tables

Figures

◀

▶

◀

▶

Back

Close

Full Screen / Esc

Printer-friendly Version

Interactive Discussion

## Photoacoustic and nephelometric spectroscopy of aerosol properties

N. Sharma et al.

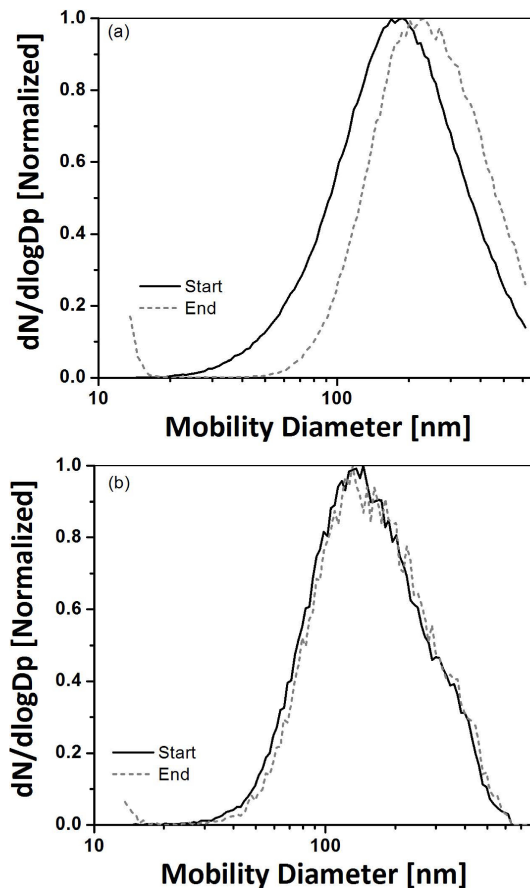


**Fig. 4.** Normalized size distribution of **(a)** soot and **(b)** salt aerosols measured by an SMPS during the experiment. The black curve indicates the initial size distribution at the beginning of the experiment and the grey dashed curve indicates the size distribution toward the end of experiment.

[Title Page](#)[Abstract](#)[Introduction](#)[Conclusions](#)[References](#)[Tables](#)[Figures](#)[◀](#)[▶](#)[◀](#)[▶](#)[Back](#)[Close](#)[Full Screen / Esc](#)[Printer-friendly Version](#)[Interactive Discussion](#)

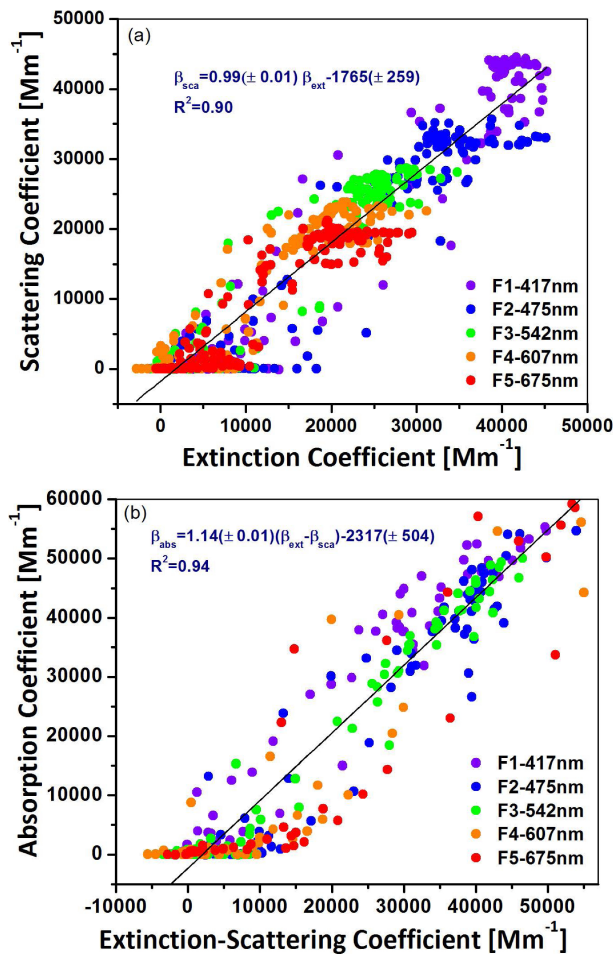


**Fig. 5.** (a) Scattering and (b) absorption calibration plots for the SC-PNS instrument at all filter wavelengths. Colors correspond to different filters.

Title Page

Abstract

Introduction

Conclusions

References

Tables

Figures

◀

▶

◀

▶

Back

Close

Full Screen / Esc

Printer-friendly Version

Interactive Discussion

## Photoacoustic and nephelometric spectroscopy of aerosol properties

N. Sharma et al.

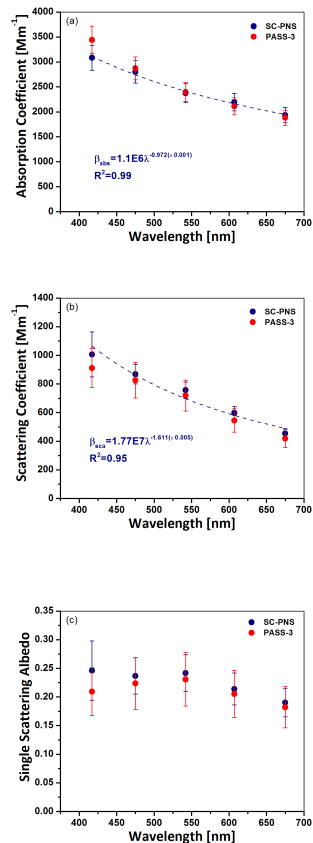


**Fig. 6.** (a) Absorption ( $\beta_{\text{abs}}$ ) and (b) scattering ( $\beta_{\text{sca}}$ ) coefficients of kerosene soot vs. wavelength ( $\lambda$ ) measured by PASS-3 and SC-PNS, error bars indicate square root of the sum of squares of background error, standard deviation of mean (standard error) and calibration variability. (c) Wavelength dependence of single scattering albedo (SSA) of kerosene soot, error bars indicate the error propagated from absorption and scattering.

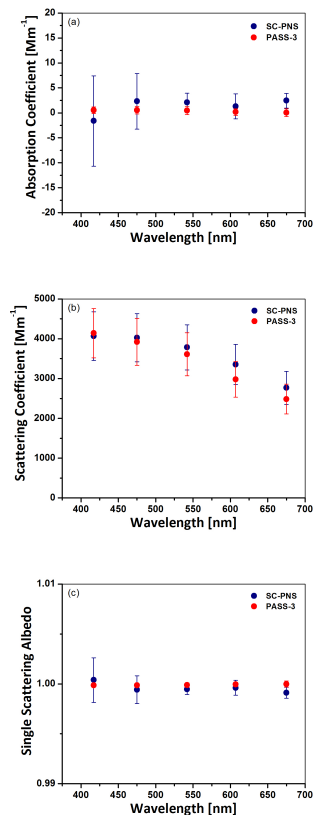


**Fig. 7.** (a) Absorption ( $\beta_{\text{abs}}$ ) and (b) scattering ( $\beta_{\text{sca}}$ ) coefficients of common salt (NaCl) vs. wavelength ( $\lambda$ ) measured by PASS-3 and SC-PNS, error bars indicate square root of sum of squares of background error, standard deviation of mean (standard error) and calibration variability. (c) Single scattering albedo of salt, error bars indicate the error propagated from absorption and scattering.

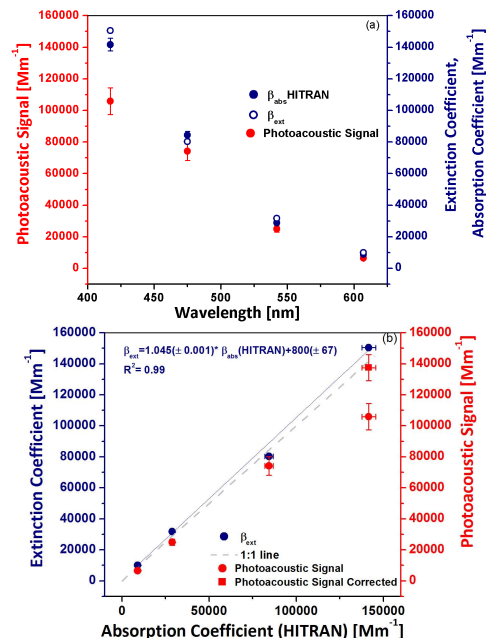


**Fig. 8.** (a) Extinction coefficient, photoacoustic signal measured by SC-PNS, and absorption coefficient estimated from the HITRAN database vs. wavelength. (b) Extinction and absorption coefficients measured by SC-PNS vs. absorption coefficients estimated from the HITRAN database. The vertical error bars on the photoacoustic signal measured and corrected for photodissociation indicate the square root of the sum of squares of the standard deviation of the mean (standard error) and the calibration variability. Vertical error bars on  $\beta_{\text{ext}}$  indicate the square root of the sum of squares of the standard deviation of the mean (standard error) and the propagated error from the laser power measurement. Horizontal errors on the absorption coefficient calculated from the HITRAN database include 2% uncertainty in  $\text{NO}_2$  absorption cross section data and 2% uncertainty in the  $\text{NO}_2$  concentration.

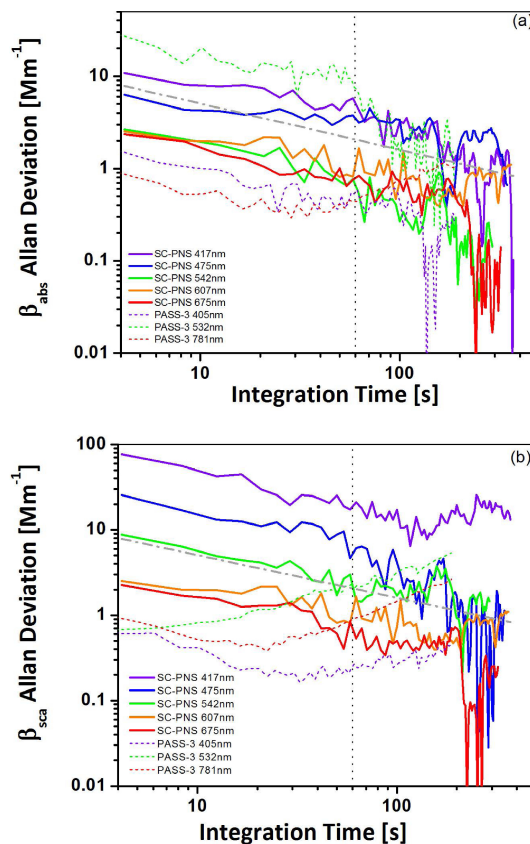


**Fig. 9.** Allan deviation vs. integration time plots for **(a)** absorption ( $\beta_{\text{abs}}$ ) and **(b)** scattering ( $\beta_{\text{sca}}$ ) coefficients at different wavelength bands for SC-PNS and at different wavelengths for PASS-3. Black dotted vertical and grey dashed lines indicate 60 s integration time and  $1/\text{square root}$  of integration time, respectively as guides to the eye.